Protein–RNA Dynamics in the Central Junction Control 30S Ribosome Assembly

Kris Ann Baker[1,†], **Rajan Lamichhane**[2,5,†], **Tek Lamichhane**[1,2,6], **David Rueda**[2,3,4] **and Philip R. Cunningham**[1]

*1 - **Department of Biological Sciences,** Wayne State University, Detroit, MI 48202, USA*
*2 - **Department of Chemistry,** Wayne State University, Detroit, MI 48202, USA*
*3 - **Section of Virology,** Department of Medicine, Imperial College London, Du Cane Road, London W12 0NN, UK*
*4 - **Single Molecule Imaging Group,** MRC Clinical Sciences Centre (CSC), Du Cane Road, London W12 0NN, UK*

***Correspondence to David Rueda and Philip R. Cunningham:** D. Rueda, Section of Virology, Department of Medicine, Imperial College London, Du Cane Road, London W12 0NN, UK; P.R. Cunningham, Office of Vice President for Research, Wayne State University, Detroit, MI 48202, USA. david.rueda@imperial.ac.uk; philc@wayne.edu*
http://dx.doi.org/10.1016/j.jmb.2016.05.010
Edited by R. L. Gonzalez

Abstract

Interactions between ribosomal proteins (rproteins) and ribosomal RNA (rRNA) facilitate the formation of functional ribosomes. S15 is a central domain primary binding protein that has been shown to trigger a cascade of conformational changes in 16S rRNA, forming the functional structure of the central domain. Previous biochemical and structural studies *in vitro* have revealed that S15 binds a three-way junction of helices 20, 21, and 22, including nucleotides 652–654 and 752–754. All junction nucleotides except 653 are highly conserved among the Bacteria. To identify functionally important motifs within the junction, we subjected nucleotides 652–654 and 752–754 to saturation mutagenesis and selected and analyzed functional mutants. Only 64 mutants with greater than 10% ribosome function *in vivo* were isolated. S15 overexpression complemented mutations in the junction loop in each of the partially active mutants, although mutations that produced inactive ribosomes were not complemented by overexpression of S15. Single-molecule Förster or fluorescence resonance energy transfer (smFRET) was used to study the Mg^{2+}- and S15-induced conformational dynamics of selected junction mutants. Comparison of the structural dynamics of these mutants with the wild type in the presence and absence of S15 revealed specific sequence and structural motifs in the central junction that are important in ribosome function.

Introduction

Ribosomes are among the largest molecular machines in all living organisms [1] and they serve as major targets for emerging peptide-based therapeutics and diagnostics [2,3]. Ribosomes assemble following a highly orchestrated process involving numerous RNA–RNA and protein–RNA interactions. Understanding the structure and dynamics of these interactions is essential for the development of novel antibiotics. During ribosome assembly, many multihelical RNA junctions function as folding nucleation sites by interacting with proteins and other regions of ribosomal RNA (rRNA) [4,5]. For example, helices 20, 21, and 22 (h20–h22, Fig. 1) form an essential three-way junction in the central domain of the bacterial 30S ribosomal subunit [6,7] that binds the primary protein S15 [8,9] (Fig. 1b). S15 has been shown to play an important role in proper 30S assembly [10–12]. *In vitro* studies have shown that the central junction is in dynamic equilibrium between an open and a closed conformation [6,7,13]. It has been proposed that S15 binding stabilizes a closed conformation, thus triggering a cascade of conformational changes that form the binding sites for other secondary central domain proteins [11,14–16]. S15 also directly interacts with Helix 34 of 23S rRNA as part of intersubunit bridge B4 [17,18].

To determine how RNA–protein interactions control 30S assembly, we have performed

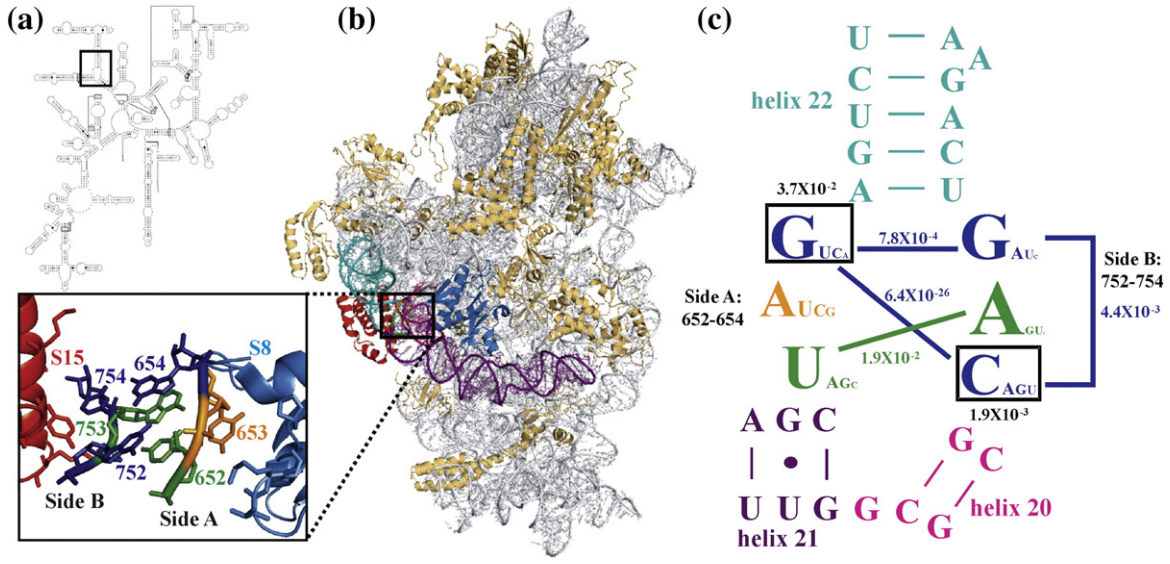

Fig. 1. Genetic analysis of the central junction. In all panels, h20 is in pink, h21 is in purple, and h22 is in cyan. (a) *E. coli* 16S rRNA; junction loop is boxed. (b) 30S subunit with the junction loop enlarged; rproteins are colored light orange and 16S rRNA is in light gray; S15 is red (Lys64, Tyr68, and Lys72 are within 2–3 Å of side-B and interact with the backbone of side-B); S8 is in light blue (Pro27, Thr54, Lys55, and Pro56 are 4–6 Å from 653); color of nucleotides indicates interactions observed in crystal structure—652:753 in green, 654:752:754 in blue, and 653 in orange [17]. (c) Analysis of selected junction clones. Font size corresponds to the proportion of isolates containing the nucleotide in the pool of selected mutants. Boxes with *p*-values indicate positions where ribosome function correlates with nucleotide identity (ANOVA) at a given position (654 and 754). Solid lines with *p*-values indicate positions that covary.

comprehensive *in vivo* genetic and *in vitro* single-molecule Förster or fluorescence resonance energy transfer (smFRET) studies. Our results identify the key sequence, structural motifs, and structural dynamics of the central junction that are responsible for proper ribosome assembly and function. Identification of these critical features provides new targets for the development of novel antimicrobials that directly or indirectly interfere with this essential conformational change in the protein synthesis machinery [19] and contribute to our general understanding of these important intermolecular interactions.

Results

Interactions between the two junction sides are required for function

To identify functionally important sequence and structural elements within the central junction, we randomly mutated nucleotides 652–654 (side-A) and 752–754 (side-B) of the *Escherichia coli* 16S rRNA junction loop (Fig. 1) using polymerase chain reaction (PCR), then we selected and analyzed the functional mutants from each side. Functional mutants from random mutagenesis of all six nucleotides comprising the central junction were isolated, analyzed, and compared to the mutants isolated from each of the individual selections to identify important interactions between nucleotides on opposite sides of the junction. The mutations were cloned in the specialized ribosome expression vector pRNA228, a derivative of pRNA123 [20–22], and expressed in *E. coli* DH5 cells; functionally active mutants were isolated by plating the transformants on medium containing 50 μg/ml of chloramphenicol and 1 mM IPTG (LBCm50).

Side-A mutations

A total of 48 side-A mutants were analyzed as described [21]. Of these, only 15 unique sequences that produce ribosomes with *in vivo* activities >10% of wild type (WT) were identified (Supplementary Table S1), indicating that transformants expressing other mutant sequences produced inactive ribosomes [21]. Analysis of the 15 survivors revealed random nucleotide distributions at positions 652 (χ^2, $p = 0.98$) and 653 (χ^2, $p = 0.87$). However, only the WT G654 nucleotide was isolated in 14 of the 15 mutants (χ^2, $p = 3.6 \times 10^{-8}$), indicating that mutations at position 654 strongly inhibit ribosome function. The 15th mutant contained U654 and produced ribosomes with only 12% activity.

Side-B mutations

We analyzed 45 side-B mutants, but only six unique sequences with >10% activity *in vivo* were

identified (Table S2). Although the sample size is insufficient for statistical analysis, it is interesting to note that each of the six mutants contained only a single mutation and that mutations were isolated at each of the randomized positions. The lowest activities observed among the mutants were C754U (16%) and C754A (11%) (Table S2), indicating that single side-B mutations strongly inhibit activity and that the effects are additive, which reduce the activity of side-B double mutants below the level required to survive the selection conditions.

Side-A and -B mutations

To identify important interactions among nucleotides on opposite sides of the junction, we simultaneously subjected positions 652–654 and 752–754 to saturation mutagenesis, and functional sequences were selected and analyzed. A total of 735 chloramphenicol-resistant transformants were isolated and 62 unique sequences (Table S3) were identified with two mutants (J1 and J2, Table S3) having <10% activity, which were excluded from further statistical analysis. All of the mutations isolated in the side-A only and side-B only selections were present in the combined mutant pool except A1 (Table S1), B1, and B2 (Table S2). If interactions between the two sides of the junction are important for ribosome function, sequences excluded during the side-A only and side-B only selections should be present among the sequences isolated when all six nucleotides were mutated. We isolated 15 sequences that were absent among the side-A survivors and 17 sequences that were absent among the side-B survivors when all six nucleotides were mutated (Table S3). In each clone, the excluded single-side sequence was accompanied by additional mutations on the opposite side. To determine if the occurrence of these sequences was due to complementation between the sides of the junction, we subcloned and assayed each of the 32 mutants in the absence of mutated nucleotides on the opposite side of the junction (Table S4). All but 4 of the 32 subclones produced inactive ribosomes (<10% of WT), indicating that interactions between the nucleotides on each side of the junction are required for ribosome function (Table S5). The four single-side mutants with >10% activity (Table S4) were added to the pool of 60 selected mutants for further analysis. Among the 64 functional junction sequences, nonrandom distributions were observed at all positions in the junction loop (χ^2, $p \leq 5.1 \times 10^{-5}$) (Table 1A). The WT nucleotide is preferred at every position except 653, at which 32 of the 64 mutations were U653A (Table 1A).

Identification of functionally important sequence and structural motifs in the central junction

Positions 654, 752, and 754

The requirement for interactions between the nucleotides on either side of the junction is supported by covariation analysis [21] (Fig. 1c). Weak but significant covariations were observed between positions 652 and 753 (χ^2, $p = 1.9 \times 10^{-2}$), 654 and 752 (χ^2, $p = 7.8 \times 10^{-4}$), and 752 and 754 (χ^2, $p = 4.4 \times 10^{-3}$), while a highly significant covariation was observed between positions 654 and 754 (χ^2, $p = 6.4 \text{ X } 10^{-26}$). Significant covariations indicate that particular nucleotide combinations occur more frequently in the pool of functional mutants than would be expected to occur by random chance. Of the 64 junction mutants, 29 contain mutations at position 654 and/or 754, 23 of which are able to form Watson–Crick (WC) base pairs. The mean activity of the 6 mutants unable to form WC base pairs is 21% ± 4.9% and the mean activity of the 23 WC pairs is 32% ± 3.4%.

Table 1. Nucleotide distribution of selected junction mutants

Nucleotide	652	653	654	752	753	754
A. Nucleotide distribution among functional mutants[a]						
A	11 [6][b]	32 [18]	5 [2]	11 [5]	**48 (27)**	11 [3]
C	6 [4]	10 [6]	9 [3]	4 [1]	2 (0)	**36 (23)**
G	9 [4]	8 [4]	**39 (24)**	**41 (24)**	7 [3]	9 [3]
U	**38 (18)**[b]	**14 (4)**	11 [3]	8 [2]	7 [2]	8 [3]
p[c]	6.2×10^{-9} (7.1×10^{-4})	5.1×10^{-5} (7.1×10^{-4})	8.2×10^{-10} (2.8×10^{-9})	1.3×10^{-11} (1.7×10^{-9})	1.3×10^{-18} (4.1×10^{-13})	2.4×10^{-7} (3.6×10^{-8})
B. Nucleotide distribution among bacteria[d]						
A	6	6345	13	17	**12,915**	10
C	11	476	10	4	5	**12,910**
G	3	803	**12,900**	**12,904**	9	7
U	**12,913**	**5309**	10	8	4	6

[a] Nucleotide distribution in 64 selected mutants with the WT sequence in bold.
[b] Numbers in parenthesis indicate the distribution of selected mutants with >40% function.
[c] Probability of random distribution based on Chi-square analysis.
[d] Nucleotide distribution in all bacterial sequences obtained from the Ribosomal Database Project from Michigan State University [34].

Thus, a WC base pair between positions 654 and 754 appears to be an important component of the central junction in functionally active ribosomes. When the nucleotide distributions were analyzed to see if the presence of particular nucleotides at a given position affects ribosome function using single-factor ANOVA, the only two positions with statistically significant ANOVAs were 654 ($p = 3.7 \times 10^{-2}$) and 754 ($p = 1.9 \times 10^{-3}$) (Fig. 1c). These findings indicate that in addition to their ability to form a WC base pair, the identity of the nucleotides forming the 654–754 pair is also important.

In crystal structures of the 30S subunit [15,17] (Fig. 1b), G654, G752, and C754 form a base triple. The presence of statistically significant covariations among these three residues (Fig. 1c) indicates that their interaction is important for ribosome function. The highly significant selection for WC pairs at positions 654:754 suggests that the weaker covariations observed between 654:752 and 752:754 (Fig. 1c) may be due to the selection of nucleotide combinations that facilitate formation of a 654:754 WC pair. Among the 64 functional mutants, 34 had mutations at 654 and/or 752, and 3 of the 34 (Table S3; clones J9, J17, J41) contained nucleotide combinations with the ability to form WC base pairs between 654 and 752. Interestingly, in all three clones, 654 also has the potential to base pair with 754, consistent with the statistically significant constraints we observed for these two residues.

Positions 652 and 753

In crystal structures, A753 stacks with A655, G654, and G588 (Fig. S1B) [17,23]. A753 is the only nucleotide in the stack from side-B of the junction, and its interaction in the stack is thought to be stabilized by the formation of a reverse Hoogsteen pair with U652 (Figs. S1B and S2A) [17,23]. A small but significant covariation (Fig. 1c) was observed between positions 753 and 652 in the pool of selected junction mutants, indicating that the interaction between them is important for ribosome function. Among the 30 mutants isolated at these two positions, 73% have the ability to form a reverse Hoogsteen pair [24]. This is only slightly more than the percentage (62%) of potential reverse Hoogsteen pairs that would be expected by random chance. The mean activity of the mutants able to form reverse Hoogsteen pairs is 41% ± 4.1% and the mean activity of the mutants unable to form reverse Hoogsteen pairs is 39% ± 7.8%. Thus, an interaction between the nucleotides at positions 652 and 753 is important for ribosome function, but no requirement for a reverse Hoogsteen pair is indicated.

As a reverse Hoogsteen pair between 652:753 is not obligatory for ribosome function, we also analyzed the effect of nucleotide identity for both 753 and 652 individually. Of the 64 selected mutants, 55 contain purines at position 753 with a mean activity of 44% ± 2.9%, and 9 are pyrimidines with a mean activity of 27% ± 6.8%. Since purines are likely to form a more stable stack than pyrimidines, these data suggest that the ability of the residue at position 753 to participate in the 655/654/753/588 stack is more important for ribosome function than its ability to form a reverse Hoogsteen pair with the nucleotide at position 652.

In 30S crystal structures, U652 not only forms a reverse Hoogsteen pair with A753, but there is also a hydrogen bond between the O4 of U652 and the 2′ OH of G752 [15,17]. A total of 26 functional mutants at 652 were isolated in the selection. The mean activity of each type of mutant does not differ by more than 5% from the 38 mutants that contain the WT nucleotide U652 (41%). Single 652 substitution mutants—A (58%), C (51%), and G (40%), (Table S3; clones J48, J42, and J30)—are about half as active as the WT. Only the WT, U652, is capable of forming both the hydrogen bond with G752 and pairing with A753; loss of either of these interactions is likely to destabilize the 655/654/753/588 stack as previously suggested [16].

Position 653

U653 is the least phylogenetically conserved nucleotide in the junction loop (Table 1B). Crystal structures [15,23] and *in vitro* S15 binding studies [16,25] suggest that it acts as a spacer nucleotide. Single substitution mutations at position 653 all have near-WT function (Table S3; clones J62, J60, and J61), but the deletion mutant (653Δ) is only 3% ± 0.5% as active as WT ribosomes, consistent with the role of 653 as a spacer nucleotide. No difference in the induction of green fluorescent protein (GFP) synthesis or the rate of growth was observed for all but the 653Δ mutant (Fig. S3).

Thirteen sets of junction mutants contain sequences that are identical except for the nucleotide at position 653 (Table S6). In each instance, the presence of U653A produced ribosomes with higher function than those with the WT U653. Additionally, 17 of 64 mutants were only selected when U653A was present in the sequence. Thus, in spite of the fact that single mutations at position 653 have little effect, U653A, in combination with other mutations in the junction, increases ribosome function. The increased function correlates with the high percentage (32 of 64) of selected functional sequences containing U653A, whereas all other positions prefer the WT nucleotide (Table 1A). Despite the prevalence of U653A, the ANOVA analysis used to determine if there is a connection between the identity of the nucleotide at position 653 and ribosome function was insignificant. This is probably due to the low function mutants that only were selected if U653A was present.

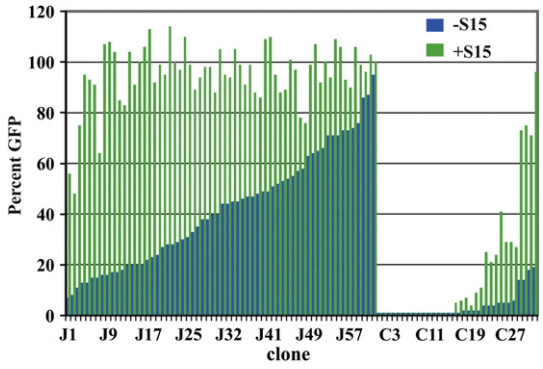

Fig. 2. S15 complementation of junction mutations. All junction mutants were assayed for ribosome function (GFP) *in vivo* in the absence (blue) or presence (green) of S15 overexpression. The data are presented as the percentage of the WT. See Tables S3 and S4 for exact percentages.

Central junction mutations affect S15 binding

The junction loop is a primary binding site for S15 [16]. To determine if loss of function in some of the junction mutants is due to decreased S15 binding, we cloned the S15 gene in the expression vector pKan5T1 T2 [26], then the 62 mutants isolated from the saturation mutagenesis of all 6 junction nucleotides (Table S3) along with the 32 single-side mutants subcloned from them (Table S4) were assayed in the presence of overexpressed S15. Of the 94 junction mutants, 78 were complemented by S15 overexpression with an increase in ribosome function of 4% to 92% (mean = 48%, Fig. 2). Interestingly, the 16 mutants that were not complemented by overexpression of S15 contained nucleotide combinations unable to form WC pairs at positions 654:754. Of the 78 complemented mutants, 61 mutants (mean function = 42% and 93% in the absence and presence of S15, respectively) have a WC pair at positions 654:754. The rest of the complemented mutants (mean function = 10% and 44% in the absence and presence of S15, respectively) contain nucleotide combinations unable to form WC pairs at positions 654:754. These results suggest a preference, but not an absolute requirement, for a WC interaction between positions 654:754 for S15 binding.

S15 binding affects 30S subunit assembly

Because S15 is a primary binding protein [10–12] and a component of an intersubunit bridge [17,18], the effect of two mutants, J12 and 653Δ (Table 2), on 70S ribosome formation was examined. Ribosomes from each mutant and the WT were prepared and separated by sucrose density gradient centrifugation in 6 mM $MgCl_2$ [21,27]. Ribosomal RNA was extracted from the 30S and 70S peaks, and primer extension was performed to determine the percentage of plasmid-derived 16S rRNA in each peak (Fig. S4 and Table 2) [21]. For each sample, the percentage of 16S rRNA in the 30S peak and the 70S peak is within experimental error (Fig. S4 and Table 2), suggesting that 30S readily associates with 50S into 70S ribosomes.

In WT cells, plasmid-derived ribosomes constitute approximately 37% of the total ribosome pool. The loss of activity in the mutants is accompanied by a decrease in the percentage of mutant ribosomes in the 30S and 70S fractions relative to the WT (Fig. S4 and Table 2). Interestingly, the decrease in plasmid-derived ribosomes in the fractions was less than the decrease in protein synthesis activity (Fig. S4 and Table 2). Overexpression of S15 in the mutants significantly increased their function (Fig. 2) and the amount of mutant ribosomes in the 30S and 70S peaks as well (Fig. S4 and Table 2). However, the increase in activity was disproportionately greater than the increase in the percentage of ribosomes in each peak (Fig. S4 and Table 2).

Table 2. Primer extension results for WT *versus* mutants

	Nucleotide sequence						S15	%	% plasmid-derived 16S in[d]:	
Clone	652	653	654	752	753	754	overexpression	function[c]	30S peak	70S peak
WT	U	U	G	G	A	C	–	100	37 ± 3	37 ± 1
							+	100	39 ± 1	36 ± 2
clone J12[a]	G	A	C	A	U	G	–	18 ± 1	13 ± 1	9 ± 1
							+	83 ± 2	23 ± 2	24 ± 1
653Δ[b]	U	Δ	G	G	A	C	–	3 ± 1	8 ± 1	9 ± 1
							+	12 ± 2	16 ± 1	14 ± 1

[a] The function of clone J12 is complemented with overexpressed S15 to near-WT levels.
[b] The function of 653Δ is only slightly complemented with overexpressed S15.
[c] The function of each mutant given as a percentage of WT function. The function is an average of at least three independent assays with standard error of the mean.
[d] Primer extension [49] was used to determine percentage of plasmid-derived 16S rRNA in 30S and 70S peaks in the presence and absence of overexpressed S15. The percentage is an average of at least three independent assays with standard error of the mean.

These data suggest that loss of function in the junction mutants is due to decreased and improper assembly of mature 30S subunits and not to failure of the mutant subunits to form 70S ribosomes.

Central junction dynamics and S15 binding control 30S subunit assembly

Previous studies have shown that the WT central junction undergoes a large conformational change that brings h20 and h22 in close proximity followed by S15 binding during ribosome assembly [6,13,15,28]. We hypothesized that the observed levels of function in the mutants are dependent on their ability to bind S15 and undergo this conformational change. To test this hypothesis, we performed *in vitro* smFRET assays (Fig. 3) [29,30] of a synthetic three-strand RNA construct that mimics the central junction (Fig. 3a) [6] with minor modifications to the h20 bulge, which do not affect S15 binding but increase RNA annealing efficiency [6,31]. The ends of h20 and h22 were fluorophore labeled and the 3′ end of h21 is biotinylated (Fig. 3a) [6], which enable real-time monitoring of the distance between h20 and h22 in the absence and presence of S15 (Fig. 3). We selected three mutants that represent the

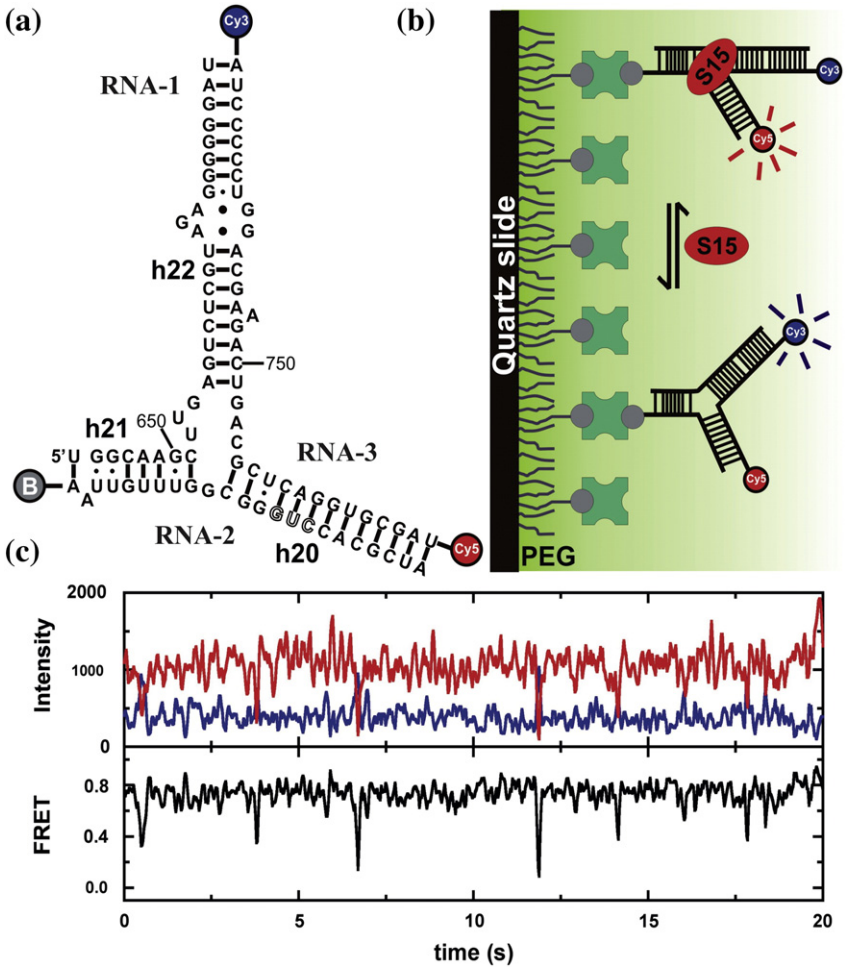

Fig. 3. Single-molecule study of the central domain junction loop of *E. coli* 16S rRNA. (a) Junction construct, with h20, h21, and h22 labeled according to the *E. coli* 16S secondary structure, is labeled with fluorophores (Cy3 and Cy5) and biotin (b). Three nucleotides near h20 were modified from the WT (GCA) sequence to increase the efficiency of annealing during the formation of the junction. (b) Schematic representation of a sample immobilization for the single-molecule experiments. The quartz slide is coated with biotin-PEG, and the biotinylated RNA sample is then immobilized through biotin–streptavidin interaction. (c) Single-molecule time trajectory of the WT junction loop in the presence of 10 nM S15 and 1 mM Mg^{2+} (donor intensity in blue, acceptor intensity in red). It should be noted that the donor alone shows no fluorescence after photobleaching (Fig. S5) and the fluorescence trajectories are corrected for crosstalk (donor emission in the acceptor channel). Also, there is no fluorescence produced for acceptor only upon excitation at 532 nm (data not shown). Lower panel is the FRET trajectory calculated from the fluorescence intensities of the donor (I_D) and acceptor (I_A) in the upper panel by using the formula FRET = $I_A/(I_A + I_D)$.

phenotypes observed in the *in vivo* genetic study (Tables S3 and S4): (i) clone J58 has three mutations but maintains a WC base pair between 654:754 and exhibits near-WT function (74%), (ii) clone J12 has all six bases mutated while maintaining a WC base pair between 654:754 but has low function (18%) that can be rescued by overexpressing S15 (83%), and (iii) clone C12 has only one mutation (G654C) that prevents the formation of the 654:754 base pair and exhibits low function *in vivo* (1%), which cannot be rescued by overexpressing S15.

The smFRET trajectories of the WT construct in absence of S15 and under near-physiological conditions (1 mM Mg^{2+} [32]) reveal that the junction adopts an open conformation with FRET values ranging between 0.4 and 0.6 (Fig. 4). A time-binned FRET histogram built from 100 trajectories reveals the presence of two major conformations centered at ~0.4 and ~0.6 FRET (Fig. 4b). Based on the time trajectories, these two conformers interchange more rapidly than our time resolution (~30 ms). Raising the [Mg^{2+}] to 10 mM results in a FRET increase to ~0.8 (Fig. 4), indicating that h20 and h22 are brought in close proximity to form the closed conformation. The corresponding smFRET trajectories reveal that the junction can still transiently enter the open conformations, which results in a second broad but minor distribution below ~0.8 FRET (Fig. 4b). Dwell time analysis of 150 time trajectories (Fig. 5a) shows that the closing rate constant (k_{close} = 9 ± 1 s^{-1}) is ~5-fold larger than the opening rate constant (k_{open} = 1.8 ± 0.1 s^{-1}), in agreement with the FRET histogram. In the presence of S15 and under near-physiological conditions (1 mM Mg^{2+}), the junction also resides primarily in the closed conformation (FRET ~0.8) with brief transitions to the open conformation (Fig. 4). The closing (k_{close} = 14 ± 1 s^{-1}) and opening (k_{open} = 1.4 ± 0.1 s^{-1}) rate constants (Fig. 5b) are similar to those measured in 10 mM Mg^{2+}, suggesting that S15 and Mg^{2+} ions may both play roles in stabilizing the closed conformation as previously suggested [6].

The clone J58 has near-WT function (74%) and is complemented to WT levels in the presence of overexpressed S15 (Table S3). This indicates that J58 would have comparable junction dynamics to the WT. However, single-molecule trajectories of clone J58 reveal that this mutant does not fold like the WT. In the absence of S15 and under 1 mM Mg^{2+}, this mutant exhibits a single conformation at ~0.4 FRET, and the fast dynamics that were observed for the WT under these conditions have disappeared (Fig. 4). Increasing the [Mg^{2+}] to 10 mM recovers the partially open ~0.6 FRET state observed for the WT but not the closed conformation (~0.8 FRET) (Fig. 4). This indicates that the junction mutations in clone J58 may have disrupted an important Mg^{2+} binding site, thus preventing the junction from folding into the closed conformation. Interestingly, 10 nM S15 with only 1 mM Mg^{2+} restores folding to the closed conformation (Fig. 4). This result shows that S15 alone can stabilize the closed conformation even when Mg^{2+} cannot.

The clone J12 is a low functional mutant (18%), which can be rescued by overexpression of S15 *in vivo* (Table S3). As observed with J58, in the absence of S15 and 1 mM Mg^{2+}, J12 smFRET time trajectories exhibit only a low FRET state (~0.4; Fig. 4), indicating that this mutant adopts primarily the open conformation. Increasing the [Mg^{2+}] to 10 or 20 mM does not result in the appearance of higher FRET species (Figs. 4 and S7), showing that Mg^{2+} ions alone cannot stabilize the ~0.6 FRET or the closed conformation. Unlike J58, time traces of J12 in the presence of 10 nM S15 and 1 mM Mg^{2+} showed few rapid transitions to the ~0.6 FRET state or the closed state (Fig. 4). The corresponding time-binned histogram of 35 trajectories shows that the ~0.6 and ~0.8 FRET states are only reached 21% and 4% of the time, respectively (Fig. 4b). Because these excursions were never observed in the absence of S15, this result shows that S15 is still capable of transiently binding the junction with lower binding affinity but fails to stabilize the higher FRET conformations. To estimate the binding affinity of S15 for J12, we increased the S15 concentration to 25 nM (1 mM Mg^{2+}, Fig. S8). Although at this S15 concentration, some of the S15 precipitated on the slide; 17 active complexes were identified and characterized, and 10 of these exhibited the closed conformation (~0.8 FRET, Fig. S8), implying that under higher concentrations, S15 binds and closes the junction, which is in agreement with the *in vivo* data.

Clone C12 is a low function mutant *in vivo* that cannot be rescued even when S15 is overexpressed (Table S4). Time trajectories of C12 in 1 mM Mg^{2+} and in the absence of S15 reveal the presence of a new static low FRET conformation (~0.2, Fig. 4). A ~0.2 FRET state indicates that h20 and h22 in the C12 mutant construct are at an angle greater than that observed in the open conformation of the junction (>120°). Increasing [Mg^{2+}] to 10 or 20 mM reveals no conformational changes showing that Mg^{2+} ions alone cannot fold the junction even into the ~0.4 FRET state (Figs. 4 and S7). Time-binned histograms of 100 time trajectories in 1, 10, and 20 mM Mg^{2+} show no discernible folding of the C12 clone junction loop (Figs. 4b and S7).

Since overexpression of S15 does not rescue the C12 clone, the expectation is that S15 cannot bind to this mutant at all. However, time trajectories in 1 mM Mg^{2+} in the presence of 10 nM S15 reveal an unexpected behavior (Fig. 4a). Time-binned histograms of 49 time trajectories show that the junction adopts the extended ~0.2 FRET conformation but briefly transitions to FRET states ranging between

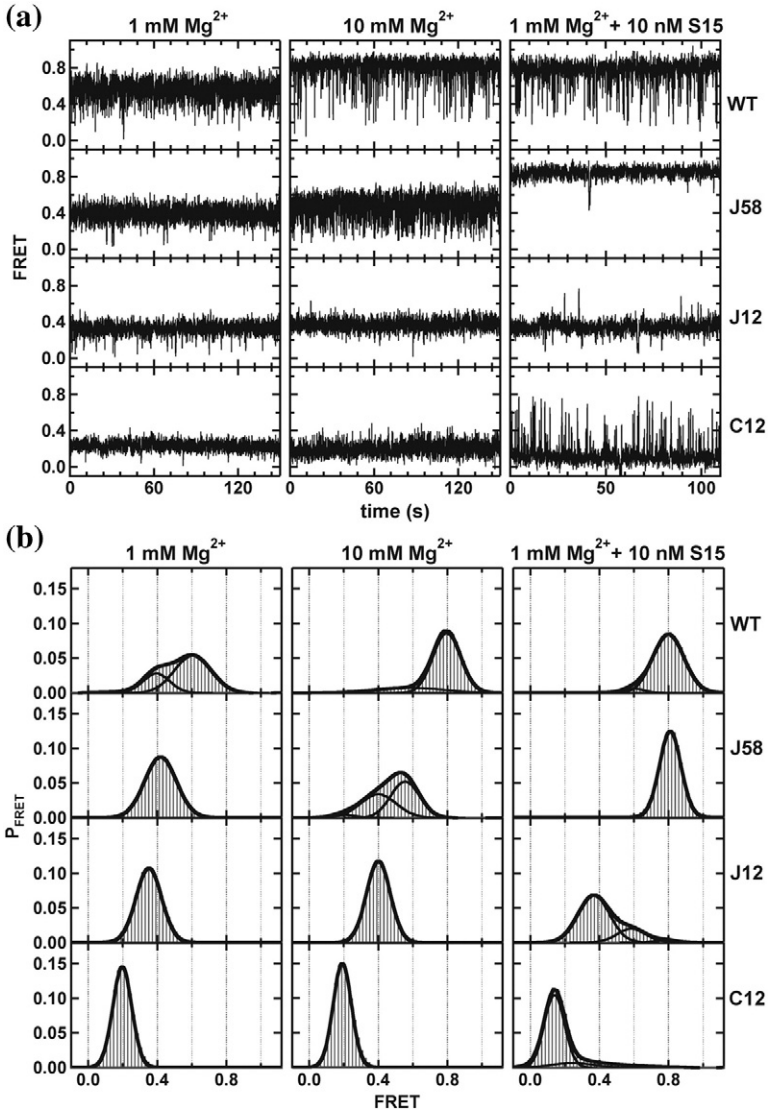

Fig. 4. smFRET trajectories and histograms reveal junction dynamics. Data points are processed with one point average after collecting them every 33 ms. (a) FRET trajectories are given for the WT and the three mutants (J58, J12, and C12) at 1 mM Mg^{2+} (left), 10 mM Mg^{2+} (center), and 10 nM S15 with 1 mM Mg^{2+} (right). (b) FRET histograms obtained from number of events at different [Mg^{2+}] in presence and absence of S15. Gaussian fit of histograms provides the distributions of molecules at each FRET state. Histograms are built with 100 molecules in each case unless otherwise mentioned in results section. At 1 mM Mg^{2+} (left), WT loop has higher events (66%) at ~0.6 and (34%) at ~0.4 states as compared to 7% and 93% at 0.5 mM Mg^{2+} (Fig. S6). At 1 mM Mg^{2+}, J58 and J12 mutants have only one distribution at ~0.4 FRET state but the C12 mutant is in ~0.2 FRET state. When the [Mg^{2+}] is increased to 10 mM (center), the distribution in the FRET histogram for WT junction loop is high (92%) at ~0.8 FRET state and 8% at lower FRET. For J58 mutant, it is shifted to ~0.6 state (58%) from ~0.4 state (38%) and the remaining 4% are in a lower FRET state. The J12 and C12 mutants do not have significant difference at this [Mg^{2+}] as compared to 1 mM Mg^{2+}. In the presence of 10 nM S15 and 1 mM Mg^{2+} (right), the WT (50 molecules) shows similar results as 10 mM Mg^{2+} (94% at ~0.8 and 6% at lower FRET states), but the J58 mutant has only one distribution at ~0.8 FRET state. The J12 mutant (35 molecules) shows three distributions: 75% at ~0.4, 21% at ~0.6, and 4% at ~0.8 FRET states. The C12 mutant (49 molecules) has two distributions: 94% at ~0.2 and 6% at higher FRET states.

~0.4 and ~0.6 (Fig. 4b). Because these excursions are never observed in the absence of S15, these dynamics indicate that S15 is still capable of binding the C12 mutant and attempts to fold it, but the ~0.4 and ~0.6 FRET conformations are destabilized by the presence of the extended stack between h20 and h22. Dwell time analysis of these transient excursions yields a $k_{close} = 2.8 \pm 0.1\ s^{-1}$ and $k_{open} = 8 \pm 1\ s^{-1}$ (Fig. 5c). These rates are opposite to what was observed for the WT junction loop under

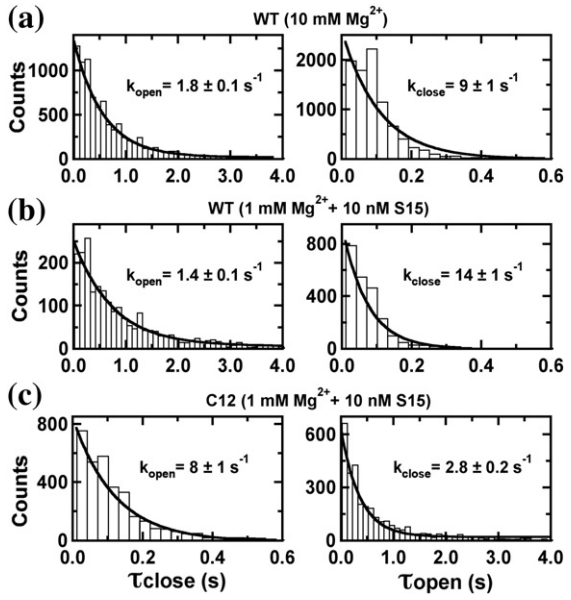

Fig. 5. Mg^{2+}- and S15-dependent single-molecule dynamics and observed rates for WT and C12 junction loops. Histograms of the number of events observed in docked (closed, left) and undocked (open, right) states. Histograms are fitted with a single exponential equation to calculate the dwell time of the open and closed states. Dwell time for the WT junction loop (a) in the presence of 10 mM Mg^{2+} and (b) in the presence of 10 nM S15 and 1 mM Mg^{2+}. Dwell time of the C12 mutant junction loop (c) in the presence of 10 nM S15 and 1 mM Mg^{2+}.

the same conditions (Fig. 5b). It is not possible to distinguish whether each excursion to the high FRET conformation corresponds to sequential protein binding events or to one S15 molecule bound for an extended period of time. However, the large magnitude of k_{close} and the high frequency of excursions suggest that each bound S15 makes multiple, unsuccessful attempts at closing the junction, while the protein remains bound to the extended junction for long periods of time (>10 s), contrary to our initial expectations. These data also indicate that S15 utilizes an induced-fit mechanism to bind the RNA junction, as shown for the L7Ae protein binding to the kink-turn motif [33].

Discussion

S15 and the central domain have become a model system for studying ribosomal protein (rprotein):rRNA interactions and the process of 30S assembly. Prior studies have been performed *in vitro* with site-directed mutations constructed in minimal binding sequences, and function was assayed by measuring S15 binding and/or monitoring changes in protection from nucleotide modification [16,25]. Here, we have combined *in vivo* genetic and functional analyses with *in vitro* biochemical and single-molecule studies to identify the sequence, structural motifs, dynamics, and molecular mechanisms involved in a critical conformational change that occurs in the central junction of the small ribosomal subunit.

The importance of structural motifs in the central junction

In 30S crystal structures [15,17], three interactions among nucleotides of the junction loop: a G654:C754 WC pair, a G752:G654:C754 base triple, and a U652:A753 reverse Hoogsteen pair (Fig. S1) are present, which are believed to aid in the maintenance of the junction structure.

Importance of the G654:C754 WC base pair

Base pairing of G654 and C754 forms an unusual structure in the junction loop (Figs. 1 and S1). To accommodate the G654:C754 base pair, the backbone of C754 twists from its standard helical shape [17,23] and the base of C754 also shifts to a *syn* configuration [15]. The changes in the backbone and the base configuration place C754 in a position to WC base pair with G654. Our results from the covariation and ANOVA analysis (Fig. 1), along with the S15 complementation study (Fig. 2), confirm that the backbone conformation created by the G654:C754 base pair [16,17,23] is recognized by S15, and this interaction of the three within the junction is the most critical for ribosome function *in vivo*.

Previous *in vitro* studies with model hairpins have shown that the mutations of the G654:C754 nucleotides, including G654C:C754G, prevent S15 binding [16] and presumably decrease ribosome function. The results of the *in vitro* studies are consistent with the conservation observed in all natural junction sequence variants (Table 1B) [4,34]. However, 654:754 mutants were identified in our *in vivo* study, but they also contain mutations at other junction nucleotides. The selection strategy used in the saturation mutagenesis was designed to isolate ribosome mutants with less than WT activity. Simultaneously changing all six of the junction nucleotides allowed the isolation of combinations that rescue the defects produced by mutating only the 654:754 pair. These junction combinations are unlikely to occur in nature since they contain multiple mutations [21,35], hence the high conservation observed for 654 and 754 in all bacteria (Table 1B) [34].

Importance of the G752:G654:C754 base triple

Nucleotide G752 forms a base triple with G654:C754 through its sugar edge [15,17,23,24] (Fig. S1). Interaction of G752 with G654:C754

provides additional stability to the junction loop structure [17,23] that is also important for optimum ribosome function. Loss of a hydrogen bond between the N2 of G752 and O6 of C754 in the single G752A mutant reduces protein synthesis by 29% *in vivo* (Table S3; clone J53). This corresponds to a 50-fold increase in K_d for S15 binding *in vitro* [16].

In the majority of junction mutants, sequences in which 654:752 could form a WC base pair were not selected. Pairing of 654 with 752 would extend h22 and disrupt the 654:754 WC pair as demonstrated in our studies with mutant C12 (Figs. 4 and 5 and Table S4). These results are also consistent with prior *in vitro* studies showing that a model junction RNA containing the G654C single mutation did not bind S15 and that both G654C and G752 had decreased reactivity to chemical modification [16]. Thus, WC base pairs between positions 654 and 752 are strongly selected against because they allow formation of a nonfunctional, alternative structure in the junction. In spite of this, three junction mutants in which 654 can pair with either 752 or 754 retained enough activity to survive selection. This creates the possibility of forming two different structures in equilibrium: one with a 654:752 pair and the other with a 654:754 pair. In part of the 30S pool, the correct structure of the central junction is formed, allowing S15 binding and the ribosome to function, but the overall function of the mutant is reduced since the entire 30S pool does not have the same activity.

Importance of the 652:753 reverse Hoogsteen pair and stacking interactions

Although crystal structures show that nucleotides 652 and 753 form a reverse Hoogsteen pair [15,17], in our mutants, the ability to form a reverse Hoogsteen pair between 652:753 is not crucial for ribosome function. The U652:A753 pair allows A753 to stack with 588, 654, and 655 (Fig. S1) [17,23]. This nucleotide stack and the U652 interaction with the 2′ OH of 752 stabilize the position of A753 [17]. The correct placement of 753 contributes to the conformation of the side-B backbone that is recognized by S15 [17], and changing the position of 753 is therefore likely to affect S15 binding. This is illustrated with the U652:A753G mutant (27%, Table S3; clone J20) that is capable of forming a reverse Hoogsteen pair, but the resulting structure would change the position of the sugar, the backbone, and the base (Fig. S2B) [24]. These alterations would possibly prevent A753G from participating in the stack with 588:654:655, which would destabilize the junction loop structure in the region that interacts with S15. This is corroborated by *in vitro* studies using a model hairpin that showed the A753G mutation resulted in 60-fold reduction in S15 binding [16]. This may also be the reason for the observed low activity of the A753U mutant (23%) (Table S3; clone J18 and Fig. 2C).

Position 653 is a spacer

Our results presented in this study for the mutagenesis of 653 (Fig. S3) are consistent with the prediction of others that the nucleotide at position 653 functions primarily as a spacer [25]. We also show that 653Δ-containing ribosomes do not assemble properly, but both the assembly and protein synthesis defects were partially restored by overexpression of S15 (Fig. S4 and Table 2). In contrast, *in vitro* studies that were performed with model RNAs showed little to no difference in S15 binding between the WT and the 653Δ mutant [13,16,25]. It is possible that the smaller 653Δ RNA was able to bind S15, although at a lower affinity, but lacked the required dynamics for 30S assembly, similar to our smFRET analyses of mutant C12 (Figs. 4 and 5 and Table S4). This suggests that, in addition to orienting junction nucleotides to maintain the required intra-junction interactions [16,23], 653 provides freedom for side-A (Fig. 1) to stretch as the junction folds.

Interestingly, in spite of the fact that all three single substitution mutations at position 653 produce ribosomes that are fully active *in vivo*, the presence of U653A in combination with other junction mutations produces ribosomes that are significantly more active than the same mutants containing U653, U653C, or U653G (Table S6). In crystal structures [17], U653 flips out of the loop into a pocket created by rprotein S8, placing U653 4–6 Å away from Pro27, Thr54, Lys55, and Pro56 of S8 (Fig. 1b). The U653A substitution creates the potential for additional contacts with S8 that stabilize the conformation of mutant junction loops to retain the conformation of the backbone required for S15 binding. The stabilizing effect of U653A on central junction structure may account for the presence of A653 in 16S rRNA of the thermophile, *Thermus thermophilus* [4]. Overexpression of S8, however, does not complement loss of function in the junction mutants (Table S7), suggesting that S8 does not participate in U653A stabilization of the junction mutants.

S15 and the junction loop

Several studies have shown that the junction loop is one of the primary S15 binding sites [16,25,31,36]. Our data showing that S15 overexpression *in vivo* restores function (Fig. 2) indicate that the junction mutations reduce the affinity of 16S rRNA for S15, which causes an assembly defect as shown by our primer extension assays of clones J12 and 653Δ (Fig. S4 and Table 2) in the absence of S15 overexpression. However, the lack of correlation between the percentage of mutant 30S and their level of function implies that the mutations produce a pool of 30S that were not all equally active. This suggests that, in a fraction of the mutant 30S, the junction helices have undergone a minor shift in

conformation that inhibited protein synthesis without affecting assembly or association. Transitions between at least two conformations were detected in our FRET experiments of clone J12 (Figs. 4 and S8), which support the idea of multiple junction structures in the pool of mutant 30S. It should be noted that we did not determine the composition of the mutant 30S and 70S, so it is unknown if any protein components including S15 are missing that would result in the observed anomaly between the level of function and the amount of 30S.

The assembly defect in the mutants can be overcome by S15 overexpression, which is indicated by higher levels of mutant 16S in each of the 30S and 70S peaks. For 653Δ, in a similar manner to assays performed in the absence of S15, a mixed pool of 30S was produced as discussed above. However, for clone J12, the increase in percentage of mutant 16S is less than the increase in function, for which there are two non-mutually exclusive explanations. The first explanation is that S15 overexpression causes a higher proportion of the mutant 30S pool to be active. The second explanation is that each mutant ribosome produces more protein than a WT ribosome. This implies a higher translation rate for the mutant in the presence of overexpressed S15. Although the junction has never been implicated in controlling the rate of translation, it is possible that the junction mutants have an indirect effect since junction folding and S15 binding affect the positioning of other nucleotides [11,14–16], such as 693 in helix 23b, that are thought to alter the translation rate [35].

In spite of the established *in vitro* assembly pathway [10,12,37] and the correlation we observed between binding of S15 and the amount of 30S, the assembly process appears to be more complex than expected. Bubunenko *et al.* previously reported that a strain with the S15 gene deleted from the genome (Δ*rpsO*) was still viable [38]. The 30S subunits isolated from the Δ*rpsO* strain have a full complement of the other rproteins, including central domain proteins: S6, S18, S11, and S21, suggesting that S15 is not essential for ribosome assembly [38], which is not supported by the results obtained in this study. Talkington *et al.* proposed that 30S subunits are capable of following several different pathways of assembly *in vivo* [39], which suggests that assembly could proceed in the absence of S15. As observed in smFRET experiments, the WT junction is able to fully transition between the open and closed conformations (this study and Ref. [6]). Even in the absence of S15 stabilizing the closed conformation, it is possible that the junction could be locked in the closed conformation by the rest of the 30S assembling through an alternative pathway in the presence of Mg^{2+} [38]. In the junction mutants with reduced Mg^{2+} binding and dynamics as shown by our smFRET experiments, the presence of S15 becomes more important for the assembly process. It should be noted that the doubling time of cultures of the Δ*rpsO* strain (90 min at 37 °C and >660 min at 25 °C) was increased as compared to a WT culture (30 min at 37 °C and 60 min at 25 °C), indicating problems with ribosome biogenesis [38]. Therefore, S15 may not be absolutely necessary, but *in vivo*, it plays a critical role in the production of an active ribosome pool and the establishment of fitness.

Junction dynamics

Ha *et al.* previously utilized smFRET and a labeled three-strand construct of helices h20, h21, and h22 to study the conformational changes of the WT junction in the presence of S15 and Mg^{2+} [6]. For control purposes, the smFRET experiment with the WT junction construct was repeated and our results are consistent with previous data indicating that Mg^{2+} and S15 both cause the same conformational change in the junction [7,13] and are comparable with studies by Ha *et al.* [6]. However, the traces we obtained with 10 mM Mg^{2+} showed quick transitions from the high to low FRET states, indicating rapid switches between the open and closed conformations (Fig. 4). Similar transitions existed in the S15 traces but were much less frequent than with Mg^{2+} (Fig. 4). Ha *et al.* determined that the K_d for Mg^{2+} (240 μM) was 80,000-fold higher than for S15 (3.5 nM) [6]. Thus, the decreased binding affinity of Mg^{2+} as compared to S15 may be the reason for the frequent transitions and the shorter dwell time in the closed conformation (Fig. 5) observed with Mg^{2+}, since it would dissociate from the junction more often than S15 [6], which makes S15 better at stabilizing the closed conformation.

Mutations that cause changes with both S15 binding and protein synthesis are likely to affect junction dynamics *in vivo*. The smFRET method developed by Ha *et al.* was adapted (Fig. 3) in the current study to investigate the dynamics of several junction mutants. Three mutants—J58, J12 and C12 (Tables S3 and S4)—were chosen based upon their *in vivo* ribosome function and their complementation by S15.

Clone J58 has 74% function *in vivo* that increases to WT levels when S15 is overexpressed (Table S3). This allowed the comparison of the dynamics of J58 to WT, but in contrast with WT, J58 exhibits significantly different behavior with Mg^{2+}. Most of the molecules were in the low FRET state (~0.4–0.5), even in 20 mM Mg^{2+} (Fig. S7), which is the FRET state observed for the WT construct in 500 μM Mg^{2+} (Fig. S6). Mg^{2+} is bound to positions 653, 752, and 753 (Fig. 1) [40]. Only one of these positions, U653A, is mutated in J58, but the other mutations, G654U and C754A, may affect the structure of the other nucleotides in the central junction. In J58, the O4 of uridine and N6 of

adenosine (O6 of guanosine and N4 of cytidine in WT), which are necessary for the G654U:C754A base pair to hydrogen bond with G752, are present. Since transversion mutations occurred at both positions, the functional groups in the mutant are most likely shifted [24]. This shift should not affect the backbone of 654 or 754, but the backbone of 752 would also have to shift to maintain interactions with the 654:754 base pair. Thus, the change in the backbone position of 752 and the mutation of 653 presumably affects the binding of Mg^{2+}, resulting in the observed inability of Mg^{2+} to stabilize the closed conformation of the central junction, and is probably responsible for the loss of ribosome function we observed in the J58 mutant *in vivo*.

Unlike the dynamics of J58 with Mg^{2+}, the presence of 10 nM S15 with 1 mM Mg^{2+} shifted the junction to a closed state more similar to the WT, consistent with the hypothesis that Mg^{2+} and S15 stabilize the junction by two separate mechanisms [13]. Direct contacts between S15 and the central junction construct rather than electrostatic interactions are mostly responsible for the stabilization of the closed conformation. A network of 15 hydrogen bonds between the RNA and S15, including contacts with side-B nucleotides 753 and 754, supports this observation [17]. Hydrogen bonds were calculated using the 30S ribosomal subunit crystal structure (Protein Data Bank accession code: 2AVY [17]) and the Swiss-PDB viewer program‡ [41].

Interestingly, in the presence of 10 nM S15 with 1 mM Mg^{2+}, there are fewer rapid transitions to the low FRET states with J58 as compared to the WT. This suggests that the binding affinity of S15 is higher for this mutant than WT (Fig. 4). These results are in contrast to our *in vivo* assays in which full activity of the J58 mutant could only be attained in the presence of excess S15 (Table S3). Ribosomal protein expression is tightly regulated and the intracellular concentration of free S15 *in vivo* is probably very low [42] and the S15 concentration in the complementation experiments is unknown. In the smFRET experiments, the majority of the molecules were in the high FRET state (~0.8), suggesting that the S15 concentration used is sufficient for full function, which accounts for the apparent discrepancy between S15 overexpression *in vivo* assays and the smFRET results.

For clone J12, results equivalent to J58 were obtained in the smFRET experiments with Mg^{2+}. In all tested concentrations of Mg^{2+} (1 mM, 10 mM, and 20 mM), the junction remained in the open conformation (~0.4 FRET) at all times. In J12, all six junction positions are mutated, including those involved in Mg^{2+} binding [40], and as with J58, this is likely to affect Mg^{2+} binding. A predominant FRET state of ~0.4 was also observed in the presence of 10 nM S15 and 1 mM Mg^{2+} (Fig. 4), but there are some excursions to the higher FRET states (~0.6–0.8) (Fig. 4). This indicates that the central junction of J12 remains in the open conformation for the majority of the time due to a decreased affinity for S15. The transitions suggest that the binding of S15 is not a stable interaction, which is consistent with our function (Table S3) and primer extension results (Fig. S4 and Table 2) for J12. The smFRET study in the presence of 25 nM S15 with 1 mM Mg^{2+} showed the closed conformation with a FRET state of ~0.8 (Fig. S8). Under these conditions, a few transitions to lower FRET states were still observed, suggesting that even in 25 nM, S15 was not stably bound, which may account for the inability of S15 complementation to restore full activity to the J12 mutant (83% with overexpressed S15). These results indicate that the binding affinity of S15 to the J12 mutant is less than that for the J58 mutant and the WT.

For the clone C12, a FRET state of ~0.2 was obtained for all tested Mg^{2+} concentrations (1 mM, 10 mM, and 20 mM) (Figs. 4 and S7). A possible explanation for this observation is that the G654C mutation prevents the formation of 654:754 base pair, in favor of the 654:752 base pair, which has also been hypothesized through the use of other central domain model structures *in vitro* [16]. This potentially allows A753 to base pair with either U653 or U652 and C754 with G587 from h20 that would cause stacking between h22 and h20 and generate a long extended helix, which would result in ~0.2 FRET (referred to as the wide-open conformation) as observed. A h22–h20 coaxial stack would prevent the formation of the h21–h22 coaxial stack seen in WT ribosomes. This would block 30S subunit assembly and probably account for the low activity of the C12 ribosomes (1%) observed *in vivo* (Table S4).

In the presence of 10 nM S15 and 1 mM Mg^{2+}, the junction is still in the wide-open conformation most of the time (Fig. 4). Unlike the experiments with Mg^{2+}, multiple rapid transitions to the higher FRET states (~0.6–0.8) were detected in the presence of S15 (Fig. 4). The calculated dwell times in the open and closed conformations imply that the junction fails to sustain the closed conformation (Fig. 5). These transitions are a consequence of the presence of S15, since they are not observed with Mg^{2+}. Although S15 has been shown to bind to the closed conformation [7,13], the transitions indicate that in C12, S15 is binding the wide-open conformation, which facilitates folding of the junction.

The smFRET construct also contains the secondary S15 binding site, a region located above the purine bulge in h22 (Fig. 1) [16]. It is possible in C12 that S15 binds to the h22 site, causing transient closing of the junction. These results differ from a footprinting experiment reported by Serganov *et al.* [16] that mutations in the junction prevented S15 binding to the h22 site. Footprinting requires S15 to bind long enough for an enzyme or hydroxyl radicals

to cleave the RNA, whereas we were monitoring junction dynamics in real-time, which may account for the apparently contrasting results. S15 binding to the C12 mutant raises the interesting possibility that dynamics of the S15–junction complex, and not protein binding alone, are important for the assembly of functional 30S ribosome subunits.

In summary, these smFRET results suggest that the junction mutants have lost the ability to (a) bind Mg^{2+}, (b) bind S15, and/or (c) shift between the open and closed conformations (Fig. 6). Loss of any of these phenotypes results in a reduction of ribosome function. Therefore, the WT junction was selected by nature as the optimal sequence for ribosome function because it balances each of these activities.

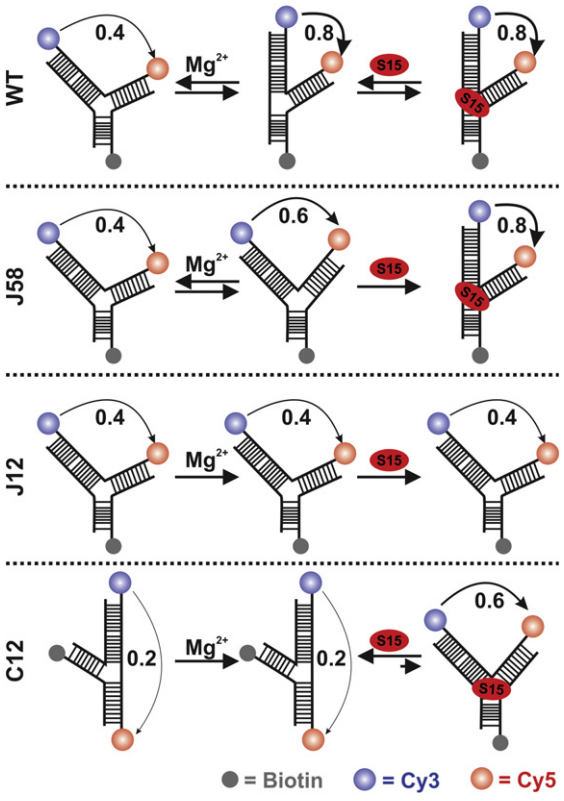

Fig. 6. Summary of the smFRET results. The effect of 1 mM Mg^{2+} (left), 10 mM Mg^{2+} (center), and 10 mM S15 plus 1 mM Mg^{2+} (right) on central junction folding is illustrated. Biotin (gray circle) is attached to h21, Cy3 (blue circle) is attached to h22, and Cy5 (red circle) is attached to h20. The arrows signify the direction of the FRET signal, and their line thickness is proportionate to the FRET values. The actual FRET values are given between the FRET dye labels next to the arrow.

Materials and methods

Bacterial strains and media

All plasmids used in mutagenesis were maintained and expressed in *E. coli* DH5 or *E. coli* GM2929 (d*am-13*::Tn *9*, *dcm-6*). Clones were cultured in LB medium containing 100 μg/mL ampicillin (LB-Amp100) and/or 30 μg/mL kanamycin (LB-Kan30). To induce synthesis of plasmid-derived rRNA from the *lacUV5* promoter, we added IPTG to a final concentration of 1 mM to LB-Amp100 (GFP induction media) at the times indicated in each experiment. Strains were transformed by electroporation. Unless otherwise indicated, transformants were grown in SOC medium [43] for 1 h prior to plating on selective medium to allow expression of antibiotic resistance genes.

Mutagenesis and selection

Construction of junction mutations in 16S rRNA

Nucleotides 652–654 were randomly mutated using PCR with primers 652N–654N and AvrII (Table S8), and the product was subcloned in pWK122, a derivative of pWK1 [44] using *Sac*I and *Bgl*II. *E. coli* GM2929 was transformed with the 652–654 pool to produce unmethylated DNA and then transferred to pRNA228, a derivative of pRNA123 [20,21] using restriction sites *Bcl*I and *BstE*II. Nucleotides 752–754 were randomly mutated using overlapping recombinant PCR with primers 752N–754N and endF (Table S8), and the PCR product was cloned in pRNA228 using *BstE*II and *Bgl*II. Mutagenesis of all six junction nucleotides was accomplished by cloning the 652–654 and 752–754 pools in pWK122 using *BstE*II and *Bgl*II, transforming into *E. coli* GM2929, and then transferring to pRNA228 using restriction sites *Bcl*I and *BstE*II.

Selection of functional mutants

Transformants from the mutant pools were incubated at 37 °C with shaking in SOC medium for 1 h to allow expression of the β-lactamase gene on the plasmid. A sample of the culture was plated on LB-Amp100 plates to determine the transformation efficiency. A final concentration of 1 mM IPTG was added to the remaining culture and it was incubated for 2 h at 37 °C for ribosome assembly and activity. The culture was then plated on LB-Amp100 + 1 mM IPTG +50 μg/mL chloramphenicol medium (LBCm50). Survivors were randomly selected, sequenced, and assayed for *in vivo* ribosome activity by measuring GFP production.

Construction of 653 deletion mutant

The 653Δ was constructed with primers 653Δ and 16S AvrII (Table S8), subcloned in pWK122, transformed into *E. coli* GM2929, and transferred to pRNA228 using restriction sites *Bcl*I and *BstE*II.

GFP assays

Overnight cultures of mutants and WT controls were grown in LB-Amp100 at 37 °C with shaking for 12–16 h. The overnight cultures were diluted 1:100 in GFP induction

media and grown at 37 °C with shaking for 24 h. After 24 h, 500 µL of the culture was pelleted, cells were washed once with 500 µL of HN buffer [20 mM Hepes (pH 7.4) and 0.85% NaCl] and resuspended in 500 µL of HN buffer. The cell suspension (100 µL) was transferred to a 96 well black, clear-bottom microtiter plate (Corning). Cell density (λ = 600 nm) was measured using a SPECTRAmax 190 (Molecular Devices, Sunnyvale, CA), and fluorescence (excitation = 395 nm and emission = 509 nm) was measured using a SPECTRAmax Gemini (Molecular Devices, Sunnyvale, CA). For each culture, fluorescence was divided by cell density and presented as a percentage of the WT. Values represent the average of at least three assays on three separate cultures done on different days.

Fluorescence induction curves

Overnight cultures of 653 single mutants were grown in LB-Amp100 at 37 °C with shaking for 12–16 h. The overnight cultures were diluted 1:500 in LB-Amp100 and incubated at 37 °C with shaking. At A_{600} = 0.1, cultures were induced with 1 mM IPTG and samples were removed for measurement of cell density and GFP analysis every 30 min. The experiment was performed only once since we also had end-point data for each mutant.

Overexpression and complementation studies

The S15 gene (*rpsO*) and the S8 gene (*rpsH*) were amplified from DH5 genomic DNA using the PCR primer pairs EcS15F + EcS15R and S8F + 8R (Table S8), respectively. Each gene was cloned into pKan5T1T2, a derivative of pKan5 [26] containing the arabinose-inducible P_{BAD} promoter and transcriptional terminators from rRNA operon B, T1T2 [45] using the *Not*I and *Xba*I restriction sites. The resulting plasmids, pKanEcS15 and pKanEcS8, were transformed into *E. coli* DH5 and confirmed by sequencing.

Complementation tests were performed by transforming *E. coli* DH5 cells containing either pKanEcS15 or pKanEcS8 with the junction mutants. Transformants were cultured on LB-Amp100 medium containing 30 µg/ml kanamycin (LB-Amp100 + Kan30). The mutant rRNA genes were induced by adding IPTG (1 mM), and the rprotein genes were induced by adding L-arabinose (0.2%).

Overexpression, ribosome preparation, and primer extension

Primer extension experiments were performed using constructs containing the C1192U mutation [46] as a stop in the WT control or the junction mutations as stops in the mutants as described by Lee *et al.* [21]. Cultures were induced with IPTG (1 mM) and L-arabinose (0.2%) at A_{600} = 0.1 and incubated until A_{600} = 0.6. Crude ribosomes were isolated from the cell pellet using standard procedures [27,47] and 30S and 70S were obtained by using a 10–30% sucrose gradient with 6 mM Mg^{2+} and centrifuging at 20,000 rpm for 15.5 h with a Surespin 630 rotor. rRNA was prepared from the 30S and 70S peaks as described in Triman *et al.* [48].

To determine the ratio of plasmid-derived 16S rRNA to host rRNA, we synthesized cDNA from the 30S and 70S extracts of each mutant and the WT using ImProII reverse transcriptase (Promega), a mix of three deoxynucleotides and one dideoxynucleotide (dependent on the mutation). The 5′-labeled primers 1192UPE, J255PE, or 653delPE (Table S8) were used to produce cDNA from WT (1192U), clone J12, and 653Δ, respectively, which were isolated by polyacrylamide gel electrophoresis and then quantified using a Typhoon imaging system and the ImageQuant program (GE Health Systems). Percentages represent the mean of three separate analyses on three separate cultures done on different days.

Production of EcS15 protein

Construction of expression vector, pET15B-EcS15

Primers 5′ pET15-EcS15 and 3′ pET15-EcS15 (Table S8) were used to amplify *E. coli rpsO* (rprotein S15) from *E. coli* DH5 genomic DNA. The product was cloned into pET15b [49–51] using *Nco*I and *Xho*I, which places S15 with an N-terminus 6X-histidine tag behind a T7 promoter, and then transformed into BL21(DE3)pLysS (*F-*,*dcm*, *ompT*, *hsdS*($r_B^- m_B^-$), *gal*, λ(*DE3*), [*pLysS* Cm^R]) [52] for protein overexpression.

Purification of 6X-histidine-tagged EcS15

An overnight culture of pET15B-EcS15 was grown in LB-Amp100 + Cm50 culture at 37 °C with shaking for 12–16 h. The culture was diluted 1:500 into four flasks of 500 mL of LB-Amp100 + Cm50 and grown at 30 °C until OD_{600} was 0.4 to 0.6. Protein expression was induced by adding 1 mM IPTG and allowing the culture to grow for an additional 16–18 h at 30 °C. The cells were pelleted at 6000 X g, resuspended in 30 mL of K-eq/wash buffer [50 mM potassium phosphate and 0.3 M KCl (pH 7)], and lysed using a French Press. Ribosomes were removed by precipitation [27], and S15 was purified from the supernatant by immobilized metal affinity chromatography using Profinity IMAC Resin (BioRad) charged with Ni^{2+}. The column-bound protein was washed with K-2W buffer [50 mM potassium phosphate, 0.3 M KCl, and 7.5 mM imidazole (pH 7)] then K-20W [50 mM potassium phosphate, 0.3 M KCl, and 20 mM imidazole (pH 7)]. S15 protein was eluted with K-E buffer [50 mM potassium phosphate, 1 M potassium chloride, and 150 mM imidazole (pH 7)]. After purification, S15 was concentrated and the imidazole was removed by filtration using an Amicon Ultra15 filter (MW: 5 kD) and by washing with K-1M buffer [50 mM potassium phosphate and 1 M KCl (pH 7)].

RNA purification and labeling

All RNA oligonucleotides were purchased from the Keck Foundation Biotechnology Resource Laboratory (Yale University, New Haven, CT) with 2′ OH protection groups. RNAs were purified and labeled as described [53,54]. Each construct consists of three RNA oligonucleotides: one is unlabeled (RNA-1), biotin is attached to the second strand (RNA-2), and donor Cy3 and acceptor Cy5 fluorophores are attached at the 5′ and 3′ ends, respectively, of the third strand (RNA-3) (Fig. 3a).

smFRET

A 1 μM solution of central junction complex was annealed by combining three RNA strands at a concentration ratio of 1:2:10 (RNA-3:RNA-1:RNA-2) in annealing buffer [10 mM NaH_2PO_4 (pH 7.2) and 20 mM NaCl]. Solution was heated to 90 °C for 45 s and slowly cooled to room temperature. Annealed junction formation was confirmed by native gel electrophoresis (not shown) [55]. Experiments were carried out with a homebuilt total internal reflection fluorescence microscope as previously described [56,57]. Biotinylated junction complex was immobilized onto PEG-passivated quartz slides via a biotin–streptavidin interaction in standard buffer [50 mM Mops (pH 7.2), 100 mM KCl, and 2 mM Trolox] at various [Mg^{2+}] [56–58] or [S15] with 1 mM Mg^{2+} as indicated in the results. Donor (I_D) and acceptor (I_A) fluorescence intensities from individual molecules were detected using an electron multiplied CCD camera. Each molecule was characterized by single-step photobleaching. Individual donor and acceptor time traces were background corrected and then used to calculate apparent FRET efficiencies as $I_A/(I_A + I_D)$ by using a custom code written in MATLAB as described previously [56,59]. FRET traces and composite FRET histograms were generated using IGOR Pro software (WaveMetrics). Dwell time analysis was performed using a custom code written in MATLAB [59] and dwell time histograms were generated and fitted using IGOR Pro.

Keywords:
16S rRNA;
ribosome protein S15;
RNA–protein interactions;
saturation mutagenesis;
smFRET

[5]Current address: R. Lamichhane, Department of Integrative Structural and Computational Biology, The Scripps Research Institute, La Jolla, CA 92037, USA.

[6]Current address: T. Lamichhane, Department of Bioengineering, University of Maryland, College Park, MD 20742, USA.

†K.A.B. and R.L. contributed equally to this manuscript.
‡http://www.expasy.org/spdbv/

Abbreviations used:
rRNA, ribosomal RNA; smFRET, single-molecule Förster or fluorescence resonance energy transfer; PCR, polymerase chain reaction; WT, wild type; WC, Watson–Crick; GFP, green fluorescent protein; rprotein, ribosomal protein.

Acknowledgments

We thank J. Williamson (The Scripps Research Institute) for constructive comments, C. Chow (Wayne State University) for the use of her lab for primer extension, C. Bedford for construction of pKanEcS15, and W. Colangelo for construction of pKanEcS8. Support from the NIH (AI061192 to P.R.C. and GM085116 to D.R.) and the NSF (MCB0747285 to D.R.) are acknowledged.

Author contributions: K.A.B., R.L., D.R., and P.R.C. designed research. K.A.B., R.L., and T.L. performed the research. K.A.B., R.L., D.R., and P.R.C. wrote the paper.

Conflict of interest: All authors declare no conflict of interest.

Appendix A. Supplementary Data

Supplementary data to this article can be found online at http://dx.doi.org/10.1016/j.jmb.2016.05.010.

Received 26 January 2016;
Received in revised form 2 May 2016;
Accepted 7 May 2016
Available online 15 May 2016

References

[1] S. Stern, T. Powers, L.M. Changchien, H.F. Noller, RNA–protein interactions in 30S ribosomal subunits: folding and function of 16S rRNA, Science. 244 (1989) 783–790.
[2] P.B. Moore, The ribosome returns, Nature. 331 (1988) 223–227.
[3] L. Otvos Jr., Peptide-based drug design: here and now, Peptide-Based Drug Design, Humana, Totowa, NJ 2008, pp. 1–8.
[4] J.J. Cannone, S. Subramanian, M.N. Schnare, J.R. Collett, L.M. D'Souza, Y. Du, et al., The comparative RNA web (CRW) site: an online database of comparative sequence and structure information for ribosomal, intron, and other RNAs: correction, BMC Bioinformatics. 3 (2002) 15.
[5] L.X. Shen, Z. Cai, I. Tinoco Jr., RNA structure at high resolution, FASEB J. 9 (1995) 1023–1033.
[6] T. Ha, X. Zhuang, H.D. Kim, J.W. Orr, J.R. Williamson, S. Chu, Ligand-induced conformational changes observed in single RNA molecules, Proc. Natl. Acad. Sci. U. S. A. 96 (1999) 9077–9082.
[7] J.W. Orr, P.J. Hagerman, J.R. Williamson, Protein and Mg(2+)-induced conformational changes in the S15 binding site of 16S ribosomal RNA, J. Mol. Biol. 275 (1998) 453–464.
[8] T. Powers, H.F. Noller, Hydroxyl radical footprinting of ribosomal proteins on 16S rRNA, RNA. 1 (1995) 194–209.
[9] P. Svensson, L.M. Changchien, G.R. Craven, H.F. Noller, Interaction of ribosomal proteins, S6, S8, S15 and S18 with the central domain of 16S ribosomal RNA, J. Mol. Biol. 200 (1988) 301–308.
[10] W.A. Held, B. Ballou, S. Mizushima, M. Nomura, Assembly mapping of 30S ribosomal proteins from *Escherichia coli.* Further studies, J. Biol. Chem. 249 (1974) 3103–3111.

[11] I. Jagannathan, G.M. Culver, Assembly of the central domain of the 30S ribosomal subunit: roles for the primary binding ribosomal proteins S15 and S8, J. Mol. Biol. 330 (2003) 373–383.
[12] S. Mizushima, M. Nomura, Assembly mapping of 30S ribosomal proteins from *E. coli*, Nature. 226 (1970) 1214.
[13] R.T. Batey, J.R. Williamson, Effects of polyvalent cations on the folding of an rRNA three-way junction and binding of ribosomal protein S15, RNA. 4 (1998) 984–997.
[14] S.C. Agalarov, J.R. Williamson, A hierarchy of RNA subdomains in assembly of the central domain of the 30S ribosomal subunit, RNA. 6 (2000) 402–408.
[15] S.C. Agalarov, G. Sridhar Prasad, P.M. Funke, C.D. Stout, J.R. Williamson, Structure of the S15, S6, S18–rRNA complex: assembly of the 30S ribosome central domain, Science. 288 (2000) 107–113.
[16] A. Serganov, L. Benard, C. Portier, E. Ennifar, M. Garber, B. Ehresmann, C. Ehresmann, Role of conserved nucleotides in building the 16S rRNA binding site for ribosomal protein S15, J. Mol. Biol. 305 (2001) 785–803.
[17] B.S. Schuwirth, M.A. Borovinskaya, C.W. Hau, W. Zhang, A. Vila-Sanjurjo, J.M. Holton, J.H. Cate, Structures of the bacterial ribosome at 3.5 A resolution, Science. 310 (2005) 827–834.
[18] G.M. Culver, J.H. Cate, G.Z. Yusupova, M.M. Yusupov, H.F. Noller, Identification of an RNA–protein bridge spanning the ribosomal subunit interface, Science. 285 (1999) 2133–2136.
[19] E. Laios, M. Waddington, A.A. Saraiya, K.A. Baker, E. O'Connor, D. Pamarathy, P.R. Cunningham, Combinatorial genetic technology for the development of new anti-infectives, Arch. Pathol. Lab. Med. 128 (2004) 1351–1359.
[20] K. Lee, C.A. Holland-Staley, P.R. Cunningham, Genetic analysis of the Shine–Dalgarno interaction: selection of alternative functional mRNA–rRNA combinations, RNA. 2 (1996) 1270–1285.
[21] K. Lee, S. Varma, J. SantaLucia Jr., P.R. Cunningham, In vivo determination of RNA structure–function relationships: analysis of the 790 loop in ribosomal RNA, J. Mol. Biol. 269 (1997) 732–743.
[22] S.V. Morosyuk, K. Lee, J. SantaLucia Jr., P.R. Cunningham, Structure and function of the conserved 690 hairpin in *Escherichia coli* 16S ribosomal RNA: analysis of the stem nucleotides, J. Mol. Biol. 300 (2000) 113–126.
[23] A. Nikulin, A. Serganov, E. Ennifar, S. Tishchenko, N. Nevskaya, W. Shepard, et al., Crystal structure of the S15–rRNA complex, Nat. Struct. Biol. 7 (2000) 273–277.
[24] N.B. Leontis, J. Stombaugh, E. Westhof, The non-Watson–Crick base pairs and their associated isostericity matrices, Nucleic Acids Res. 30 (2002) 3497–3531.
[25] R.T. Batey, J.R. Williamson, Interaction of the *Bacillus stearothermophilus* ribosomal protein S15 with 16S rRNA: II. Specificity determinants of RNA–protein recognition, J. Mol. Biol. 261 (1996) 550–567.
[26] J.H. Yeom, K. Lee, RraA rescues *Escherichia coli* cells over-producing RNase E from growth arrest by modulating the ribonucleolytic activity, Biochem. Biophys. Res. Commun. 345 (2006) 1372–1376.
[27] G. Spedding, Isolation and analysis of ribosomes from prokaryotes, eukaryotes, and organelles, in: G. Spedding (Ed.), Ribosomes and protein synthesis: A Practical Approach, IRL Press at Oxford University Press, New York, NY 1990, pp. 1–29.
[28] W. Li, B. Ma, B.A. Shapiro, Binding interactions between the core central domain of 16S rRNA and the ribosomal protein S15 determined by molecular dynamics simulations, Nucleic Acids Res. 31 (2003) 629–638.
[29] J.W. Hardin, C. Warnasooriya, Y. Kondo, K. Nagai, D. Rueda, Assembly and dynamics of the U4/U6 di-snRNP by single-molecule FRET, Nucleic Acids Res. 43 (2015) 10,963–10,974.
[30] K.S. Karunatilaka, D. Rueda, Single-molecule fluorescence studies of RNA: a Decade's progress, Chem. Phys. Lett. 476 (2009) 1–10.
[31] R.T. Batey, J.R. Williamson, Interaction of the *Bacillus stearothermophilus* ribosomal protein S15 with 16S rRNA: I. Defining the minimal RNA site, J. Mol. Biol. 261 (1996) 536–549.
[32] K.S. Karunatilaka, A. Solem, A.M. Pyle, D. Rueda, Single-molecule analysis of Mss116-mediated group II intron folding, Nature. 467 (2010) 935–939.
[33] B. Turner, S.E. Melcher, T.J. Wilson, D.G. Norman, D.M. Lilley, Induced fit of RNA on binding the L7Ae protein to the kink-turn motif, RNA. 11 (2005) 1192–1200.
[34] J.R. Cole, B. Chai, T.L. Marsh, R.J. Farris, Q. Wang, S.A. Kulam, et al., The ribosomal database project (RDP-II): previewing a new autoaligner that allows regular updates and the new prokaryotic taxonomy, Nucleic Acids Res. 31 (2003) 442–443.
[35] S.V. Morosyuk, J. SantaLucia Jr., P.R. Cunningham, Structure and function of the conserved 690 hairpin in *Escherichia coli* 16S ribosomal RNA. III. Functional analysis of the 690 loop, J. Mol. Biol. 307 (2001) 213–228.
[36] A.A. Serganov, B. Masquida, E. Westhof, C. Cachia, C. Portier, M. Garber, et al., The 16S rRNA binding site of *Thermus thermophilus* ribosomal protein S15: comparison with *Escherichia coli* S15, minimum site and structure, RNA. 2 (1996) 1124–1138.
[37] M.I. Recht, J.R. Williamson, Central domain assembly: thermodynamics and kinetics of S6 and S18 binding to an S15–RNA complex, J. Mol. Biol. 313 (2001) 35–48.
[38] M. Bubunenko, A. Korepanov, D.L. Court, I. Jagannathan, D. Dickinson, B.R. Chaudhuri, et al., 30S ribosomal subunits can be assembled *in vivo* without primary binding ribosomal protein S15, RNA. 12 (2006) 1229–1239.
[39] M.W. Talkington, G. Siuzdak, J.R. Williamson, An assembly landscape for the 30S ribosomal subunit, Nature. 438 (2005) 628–632.
[40] T. Crety, T.E. Malliavin, The conformational landscape of the ribosomal protein S15 and its influence on the protein interaction with 16S RNA, Biophys. J. 92 (2007) 2647–2665.
[41] N. Guex, M.C. Peitsch, SWISS-MODEL and the Swiss-PdbViewer: an environment for comparative protein modeling, Electrophoresis. 18 (1997) 2714–2723.
[42] C. Portier, L. Dondon, M. Grunberg-Manago, Translational autocontrol of the *Escherichia coli* ribosomal protein S15, J. Mol. Biol. 211 (1990) 407–414.
[43] D. Hanahan, Studies on transformation of *Escherichia coli* with plasmids, J. Mol. Biol. 166 (1983) 557–580.
[44] W.J. Krzyzosiak, R. Denman, P.R. Cunningham, J. Ofengand, An efficiently mutagenizable recombinant plasmid for *in vitro* transcription of the *Escherichia coli* 16S RNA gene, Anal. Biochem. 175 (1988) 373–385.
[45] J. Brosius, T.J. Dull, D.D. Sleeter, H.F. Noller, Gene organization and primary structure of a ribosomal RNA operon from *Escherichia coli*, J. Mol. Biol. 148 (1981) 107–127.
[46] C.D. Sigmund, M. Ettayebi, A. Borden, E.A. Morgan, Antibiotic resistance mutations in ribosomal RNA genes of *Escherichia coli*, Methods Enzymol. 164 (1988) 673–690.

[47] T. Powers, H.F. Noller, A functional pseudoknot in 16S ribosomal RNA, EMBO J. 10 (1991) 2203–2214.
[48] K. Triman, E. Becker, C. Dammel, J. Katz, H. Mori, S. Douthwaite, et al., Isolation of temperature-sensitive mutants of 16S rRNA in *Escherichia coli*, J. Mol. Biol. 209 (1989) 645–653.
[49] F.W. Studier, B.A. Moffatt, Use of bacteriophage T7 RNA polymerase to direct selective high-level expression of cloned genes, J. Mol. Biol. 189 (1986) 113–130.
[50] F.W. Studier, A.H. Rosenberg, J.J. Dunn, J.W. Dubendorff, Use of T7 RNA polymerase to direct expression of cloned genes, Methods Enzymol. 185 (1990) 60–89.
[51] A.H. Rosenberg, B.N. Lade, D.S. Chui, S.W. Lin, J.J. Dunn, F.W. Studier, Vectors for selective expression of cloned DNAs by T7 RNA polymerase, Gene. 56 (1987) 125–135.
[52] B.A. Moffatt, F.W. Studier, T7 lysozyme inhibits transcription by T7 RNA polymerase, Cell. 49 (1987) 221–227.
[53] D. Rueda, N.G. Walter, Fluorescent energy transfer readout of an aptazyme-based biosensor, Methods Mol. Biol. 335 (2006) 289–310.
[54] S. Wood, D. Rueda, Fluorescence labeling of nucleic acids, in: G.K. Roberts (Ed.), Encyclopedia of Biophysics, Springer, Berlin Heidelberg 2013, pp. 809–812.
[55] R. Lamichhane, G.M. Daubner, J. Thomas-Crusells, S.D. Auweter, C. Manatschal, K.S. Austin, et al., RNA looping by PTB: evidence using FRET and NMR spectroscopy for a role in splicing repression, Proc. Natl. Acad. Sci. U. S. A. 107 (2010) 4105–4110.
[56] R. Lamichhane, A. Solem, W. Black, D. Rueda, Single-molecule FRET of protein–nucleic acid and protein–protein complexes: surface passivation and immobilization, Methods. 52 (2010) 192–200.
[57] R. Zhao, D. Rueda, RNA folding dynamics by single-molecule fluorescence resonance energy transfer, Methods. 49 (2009) 112–117.
[58] T. Ha, I. Rasnik, W. Cheng, H.P. Babcock, G.H. Gauss, T.M. Lohman, S. Chu, Initiation and re-initiation of DNA unwinding by the *Escherichia coli* Rep helicase, Nature. 419 (2002) 638–641.
[59] X. Zhuang, H. Kim, M.J. Pereira, H.P. Babcock, N.G. Walter, S. Chu, Correlating structural dynamics and function in single ribozyme molecules, Science. 296 (2002) 1473–1476.